Available online at www.sciencedirect.com
ScienceDirect
Energy Reports 7 (2021) 149–162
www.elsevier.com/locate/egyr

Tmrees, EURACA, 28 to 30 May 2021, Athens, Greece

Catalytic performance of Co, Fe on MCM-41 synthesized from illite waste for gasification of torrefied cassava rhizome

Punchaluck Sirinwaranon[a], Viboon Sricharoenchaikul[b], Duangduen Atong[a,*]

[a] *National Metal and Materials Technology Center (MTEC), National Science and Technology Development Agency (NSTDA), Thailand Science Park, Pathum Thani, 10120, Thailand*

[b] *Faculty of Engineering, Department of Environmental Engineering, Chulalongkorn University, Bangkok, 10330, Thailand*

Received 28 July 2021; accepted 7 August 2021

Abstract

The catalytic gasification of torrefied cassava rhizome (TCR) with metals (Co, Fe) on MCM-41 was studied throughout this work. The focus of this research is to synthesize, evaluate and analyze the performance of ordered mesoporous MCM-41 employing illite clay waste as silica and aluminum sources under hydrothermal pressure condition using cetyltrimethylammonium bromide as structure template. The characterization of catalysts was carried out by low angle X-ray diffraction (XRD), scanning electron microscope (SEM), transmission electron microscopy (TEM), and N_2 physisorption isotherm which indicated the formation of well-ordered MCM-41 mesoporous materials, high surface area (952 m^2/g) and corresponds to a type IV isotherm of hysteresis loop, respectively. Co and Fe were deposited on synthesized MCM-41 surface by impregnation method. The catalytic performance was tested in an ex-situ gasification process at 700 °C. The 5Co/MCM-41 catalyst significantly increased the carbon conversion from 68.63% to 77.30% while using 5Fe/MCM-41 catalyst yielded the highest H_2/CO ratio of 0.66, hydrogen conversion of 26.80% and gas heating value of 10.72 MJ/kg. The results indicated that the illite waste may be converted to high-value zeolite material while TCR is a potential greener fuel feedstock for gasification. This novel method to synthesize the MCM-41 from illite clay waste utilized doping of cobalt and iron metal catalyst to increase the efficiency of gasification of TCR.

Peer-review under responsibility of the scientific committee of the Tmrees, EURACA, 2021.

Keywords: Cassava rhizome; Cobalt loaded; Iron loaded; Illite; Torrefaction

* Corresponding author.
E-mail address: duangdua@mtec.or.th (D. Atong).

https://doi.org/10.1016/j.egyr.2021.08.100

Peer-review under responsibility of the scientific committee of the Tmrees, EURACA, 2021.

Nomenclature

CV	Calorific value
CGE	Cold gas efficiency
EDX	Energy dispersive X-ray
ER	Equivalence ratio
HHV	Higher heating value
LHV	Lower heating value
MCM-41	Mobil Composition of Matter No. 41
P/P_0	Relative pressure
S_{BET}	Specific surface area determined by gas adsorption method
SEM	Scanning electron microscope
TEM	Transmission electron microscope
TCR	Torrefied cassava rhizome
XRD	X-ray powder diffraction

1. Introduction

Lignocellulosic materials, principal biomass among alternative energy field, can be converted directly into biofuels (syngas, liquid fuels, and biochar) by pyrolysis and gasification. Using various types of biomass fuel such as cassava rhizome, wood, corncob, palm, and coconut shell are suitable feedstock for these processes [1,2]. As described by Encyclopædia Britannica, cassava rhizome is also called creeping rootstalk, a horizontal underground stem which can send out both shoots and roots. Fig. 1, cassava rhizome is the connection part between stem and ground roots which is biomass residues from harvesting or starch manufacturing. After finished harvest, the cutting stem about 20 cm long was used for new plantation. Therefore, a lot of cassava rhizome was abandoned in field (8–9 million ton/year). Typically, it is burnt by farmer which is not only effect on the environment but also loss of potential energy source. In fact, the content of carbon and calorific value (CV) of cassava rhizome are suitable for synthesis gas production via gasification. Unfortunately, the inherent drawbacks of cassava rhizome are varied quality, low bulk density, low net energy density, low calorific value, hydrophilic, moisture absorption, and short shelf life. The torrefaction or mild pyrolysis is a preferred method for upgrading biomass properties for energy source. This process can promote the quality of biomass solid fuel by heating them around 200–300 °C under dry and non-oxidative (N_2 or CO_2) [3–6] or oxidative (air, flue gas) [7,8] atmospheres. Several researchers found that torrefaction is an upgrading technology to elevate physicochemical properties of biomass, for example, the torrefied solid product has several advantages and better-quality solid fuel because of its net energy density, higher calorific value [9], lower atomic ratio of oxygen to carbon (O/C) and hydrogen to carbon (H/C) [10], improving in hydrophobicity [11], better grindability [12]. Although, torrefied biomass is the potential application in gasification and energy production, tar (light or higher molecular hydrocarbons) and low gas products during the gasification process are still the main challenges of processing the raw gas. The operating parameters in gasification process such as gasifying agent (steam, oxygen, or air), operating temperature, pressure, gasifier design, and various catalysts on gasification have been experimented for tar reduction [13,14].

Zeolite materials for catalytic gasification have promising features which are not only reduce the tar components in the fuel gas, but also enhance the fuel gas quality. However, the drawback of using synthetic zeolite preparation from commercial silica source are high cost and toxicity [15]. To overcome the problem, many researchers prepared alternative raw materials for zeolite synthesis via hydrothermal method. Broad spectrum of geological materials (soils, clay, rocks and sediments) and industrial wastes such as kaolin clay, oil shale ash, bagasse fly ash, lithium slag, and waste aluminum cans may be utilized and converted into zeolite namely LTA, Na-P2, Na-X and Na-A, FAU/LTA, and LTA, respectively [16–20]. The results indicated that changing of the silicon source influenced crystallite size and morphology which in turn significantly improved catalytic activities of such mesoporous materials. The aluminosilicate source such as wheat stem ash, coal fly ash, natural clay and iron ore tailing have been utilized as a MCM-41 precursor which are widely used as adsorbent the phosphate, cesium ions, and organic contaminates in wastewater, respectively [21–24]. However, synthesized MCM-41 shows large pore volume, narrow pore size

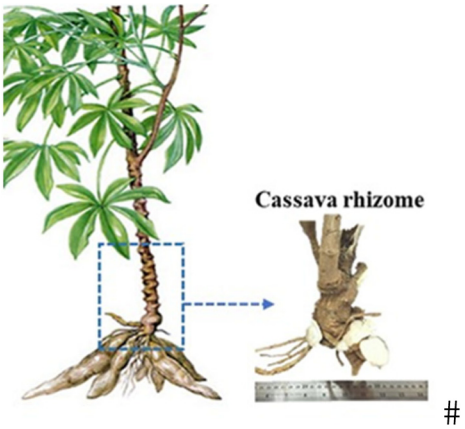

Fig. 1. Cassava rhizome biomass.

distributions, pore arrangement order and high surface area which are very important properties for catalytic biomass gasification.

Large amounts of illite wastes are generated by illite mining and dressing which takes part in 70 wt% of raw illite clay. There are ubiquitous clay mines in Thailand of which 64 mines are actively operating with yield of more than 420,165 tons clay product leading to continuous illite waste disposal without just economic utilization and cause environmental problem. Illite clay shows low pozzolanic properties, so the heat treatment at the range of high temperatures (above 930 °C) both pure mineral with small mixtures were performed for interstratified [25]. Up to present, the mixing of illite-chlorite and illite-smectite for pozzolanic reaction in a blended cement for good strength cementitious material were reported by Garg and Skibsted (2016) [26], and Irassar et al. (2019) [27]. There are only few studies about the illite waste utilized as MCM-41 precursor. In fact, illite waste whose benefits are low-cost, simplicity in handling, and regenerability can also be served as an aluminum (Al) and silicon (Si) source for a synthesis of MCM-41 zeolite.

Biomass gasification products can be improved by nickel (Ni), cobalt (Co) and iron (Fe) based catalysts. Ni-based catalyst is proved to be effective for cracking of C–C, C–H and O–H bonds during the tar reforming with limitations from quickly deactivate and cover by solid coke formation and sintering its active sites [28]. Recently, cobalt oxide was successfully incorporated with forming of cobalt oxide on the silica walls. Co-based catalysts have superior stability, higher selectivity of heavy hydrocarbon and hydrogenation, and lower water–gas shift activity, while Fe-based catalysts exhibit a significant reduction of tar and relatively high stability towards coke deactivation on surface, high water–gas shift activity and an advantage of lower price [29,30]. In our previous study, torrefied cassava rhizome (TCR) under simulated flue gas atmosphere showed good ability to enhance solid fuel properties such as lower atomic ratio of O/C, and when gasified, TCR generated lower carbon dioxide (CO_2). Addition of nickel catalyst supported on MCM-41 improved the biomass gasification efficiency [31]. The aim of this work is to effectively gasify TCR with Co and Fe on a green MCM-41 synthesized from illite waste.

2. Experimental

In this work, the experimental procedure consists of 3 parts; (i) synthesis of MCM-41 catalyst by chemical route of which the reaction mechanism has been studied thoroughly and well-comprehensible among researchers for their physio-chemical properties and subsequently the application for illite waste part. (ii) synthesis MCM-41 from illite waste as support of Co and Fe (iii) gasification of torrefied CR fuel with cobalt and iron catalyst supported on MCM-41 catalysts.

2.1. Synthesis of MCM-41 zeolite (chemical route)

MCM-41 mesoporous was prepared by adding tetra ethyl orthosilicate (TEOS. 98%, Aldrich Chem Co) as silica source and cetyltrimethylammonium ammonium bromide (CTAB, 99%, Aldrich Chem Co) as a template

for the honeycomb-liked micelle arrays structure. The solvents, demineralized water, ethyl alcohol, and ammonium hydroxide were used for inducing the hydrolysis of TEOS. The first step, CTAB was dissolved in demineralized water and mixed with ethyl alcohol and continuously stirred at 25 °C for half an hour. The ammonium hydroxide solution was carefully added to the TEOS solution and agitated for another 2 h. The liquid mixture was controlled at the pH of 10–11 by using acetic acid and left aging for 24 h, then the mixture was filled in the Polytetrafluoroethylene-lined and stainless-steel jacket hydrothermal autoclave reactor and heated at condition of: 100 °C for 48–72 h, 110 °C for 48–72 h, and 12 °C for 48–72 h. The precipitated powder product was filtered and repeatedly purged with demineralized water by the vacuum system. For template removal, MCM-41 powder was dried and pulverized and then calcined in stagnant air at 540 °C for 4 h with ramping rate of 1 °C/min. Synthesized MCM-41 presents as a white powder with relatively low density which lends from it a characteristically fluffy texture when handled.

2.2. Synthesis of MCM-41 from illite waste and preparation of Co and Fe on MCM-41

The illite waste particle size in this work was selected in range of 125–425 μm because this size does not meet the quality standard to sell as a clay product. The synthesis of MCM-41 from illite waste for mesoporous silica (Si/Al ratio = 42 and 59) was achieved by following the condition of chemical route methodology. This part consists of extraction of silica from illite waste and preparation of Co and Fe on MCM-41 supporter (Co/MCM-41 and Fe/MCM-41). First, sodium hydroxide (NaOH) powder was mixed with the illite waste sample at weight ratio 1.2:1 and fused at 550 °C for 60 min with temperature increasing rate of 1 °C/min. Silica precursor (supernatant solution) was prepared by dissolving the green powder with demineralized water for weight ratio of 1:4 for 24 h and magnetic agitation subsequently. Then 3.45 g of CTAB was dispersed in 45 ml of demineralized water. Ammonium hydroxide of 5.40 ml were combined and agitated at 25 °C for 30 min. Stirring of TEOS (8.30–9.30 ml) was continued until heterogeneous gels become homogeneous mixture, with pH of 10.5–11 adjusted by addition of acetic acid for 24 h. The composition of synthesized material is $1SiO_2$: 0.25CTAB: $2.8NH_4OH$: $93H_2O$ and subjecting to hydrothermal process. The MCM-41 powder for metal loading after calcination is obtained as the final product.

Cobalt and iron on MCM-41 supporter were prepared by impregnation method. Inorganic compound as metal salt with the formular of $Co(NO_3)_2$ $.6H_2O$ and $Fe(NO_3)_3{\cdot}9H_2O$ were dissolved in ethyl alcohol for 10 min. The MCM-41 powder was conveyed into the precursor solution and agitated for 4.5 h then the liquid substance was evaporated at 55 °C by vacuum rotary evaporator. The solid powders were obtained by calcination at 550 °C for 4 h with temperature increasing rate of 1 °C/min in stagnant air. The characterization structure of synthesized MCM-41 mesoporous were derived and confirmed by; (1) X-ray diffractometer using Cu-Kα radiation (2) The Brunauer–Emmett–Teller (BET) method for the external and internal specific surfaces area of a porous material via nitrogen physisorption, (3) Scanning electron microscopy (SEM) for structural analysis of MCM-41, (4) Transmission Electron Microscope (TEM) for surface morphological study. The following sections discuss in detail the results of physical characterization for selected synthesized MCM-41 samples.

2.3. Catalytic gasification system

The ex-situ catalytic gasification were tested in this work using TCR size 0.425–0.850 mm as raw material. The initial step in the thermochemical conversion of biomass was accomplished in a downflow reactor, and the volatile and gas products were undergone catalytic upgrading in the secondary reaction vessel. The char deposits inside of reactor while the volatilized products, tar and vapors pass through the catalyst stage for reforming. The diagram of gasification system was illustrated in Fig. 2. During gasification process at 700 °C, TCR was continuous entered into the reactor as rate of 1.0 g/min for a period of 30 min. The ratio of N_2 and O_2 carrier gas was modified to achieve equivalence ratio (ER) of 0.4. K-type thermocouples were placed throughout the reactor, and at catalytic vessel. In this work, silicon carbide (SiC), whose intrinsic properties are superior thermal properties and chemical inertness, was mixed with the catalyst at the weight ratio of 55:1. The catalytic stage temperature was set at 500 °C. The liquid and tar product were collected and trapped in a unit of condenser. After separation of condensate, produced gas in pipeline was filtered and measured by glass wool and volumetric gas meter, respectively. Gas samples were sampling drawn by peristaltic pump into a clean-up gas unit for composition analysis using online gas analyzer (Gasboard-3100p instrument) which measured the concentration in the major gas (H_2, CO, CO_2, CH_4, and C_xH_y with TCD).

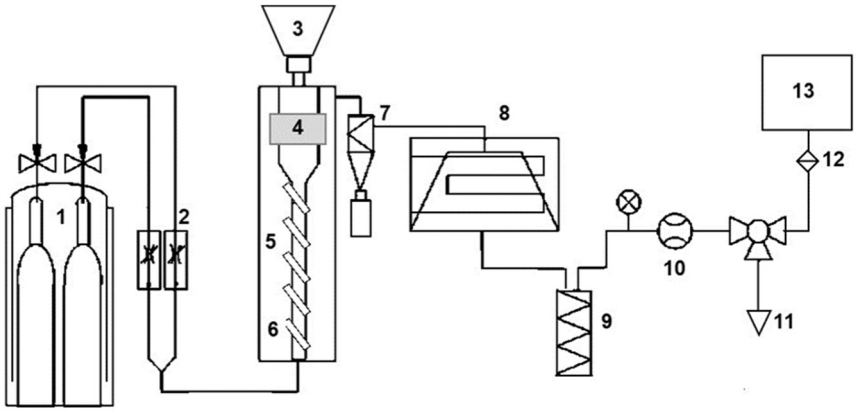

Fig. 2. Schematic of catalytic gasification experiment: (1) carrier gas (2) rotameter (3) feeder (4) catalyst stage (5) electrical furnace (6) downflow reactor (7) cyclone (8) condenser (9) gas washers (10) volumetric gas meter (11) vent (12) gas filter (13) online syngas analyzer.

3. Results and discussion

3.1. Analysis of MCM–41synthesis (chemical route)

Synthesized MCM-41 presents as a white powder with relatively low density which lends it a characteristically fluffy texture when handled. In this sense, it is quite similar to fumed silica. MCM-41 materials are formed by electrostatically interaction between the CTAB (cationic surfactant) and TEOS (silica polyanions). The surfactant template removed materials by calcination, the mesoporous material is obtained with pore diameter approximately 2 to 5 nm. A low angle X-ray diffractometer pattern (Rigaku TTRAX III) for a calcined MCM-41 sample, prepared by the chemical (TEOS and CTAB) synthesis batch, is presented in Fig. 3. A complete set of low angles XRD patterns appeared for all MCM-41 synthesized samples. The low angles XRD pattern for a well-formed example of MCM-41 displays a minimum of three prominent peaks between 0.5–8 degrees. These four peaks are labeled (d_{100}), (d_{110}), (d_{200}) and (d_{210}) according to the Miller–Bravais indices of the hexagonal unit cell.

The removal of CTAB from the inside of the pores by calcination at temperature of 550 °C led to mesoporous MCM-41 with high total specific surface area of approximately 997–1,051 m^2/g and pore diameter distribution in the range of ca. 3.00 to 3.30 nm for all samples (Table 1). The SEM and TEM of some MCM-41 synthesized

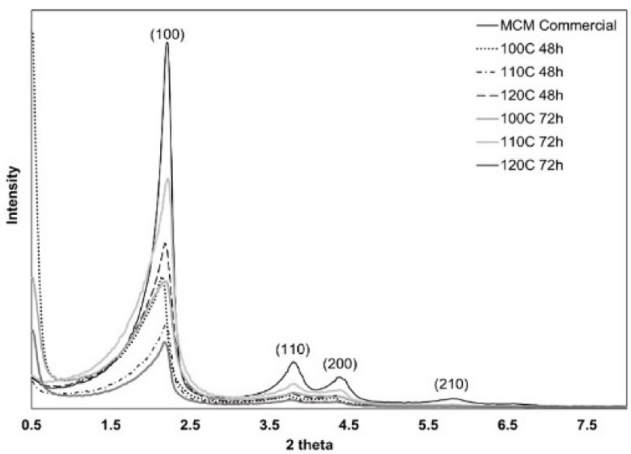

Fig. 3. Powder X-ray diffraction patterns (crystallinity) of MCM-41 synthesized by chemical route.

Table 1. Properties of chemical route synthesized catalysts.

Catalyst sample	S_{BET} (m^2/g)	Pore diameter (nm)	Pore volume (cc/g)	Wall thickness (nm)
MCM-41(Commercial)	1064	2.71	0.91	1.90
Chemical synthesis				
100 °C 48 h	1051	3.19	0.92	1.48
100 °C 72 h	1048	3.27	0.87	1.38
110 °C 48 h	1036	3.20	0.99	1.47
110 °C 72 h	999	3.14	0.79	1.57
120 °C 48 h	975	3.17	0.94	1.58
120 °C 72 h	997	3.04	0.84	1.63

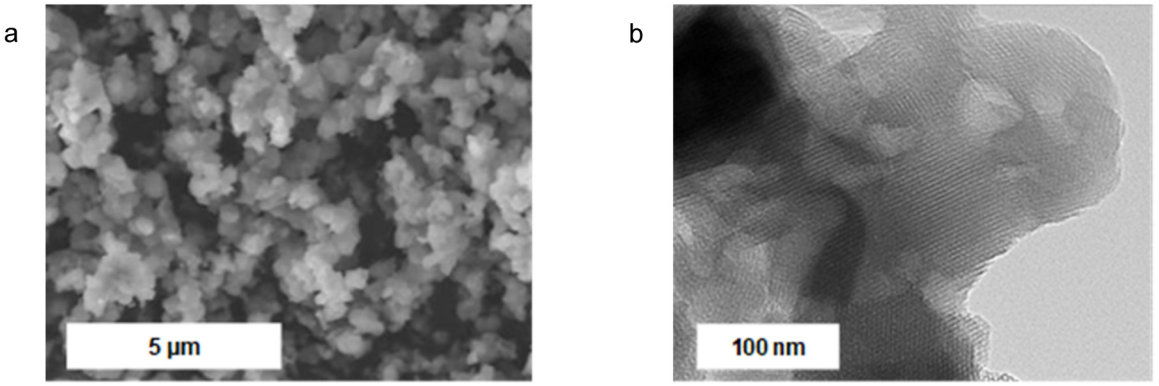

Fig. 4. (a) SEM and (b) TEM images of synthesized MCM-41.

samples were exhibited in Fig. 4. SEM image (Fig. 4a) shown the presence of MCM-41 mainly had an irregular spherical particle shapes which are a typical feature of mesoporous materials. All the materials obtained at pH = 10.5, show well defined ordered two-dimension regular hexagonal arrays of mesopores with long-range uniform cylinder shape of MCM-41 materials (Fig. 4b). The correspondence between the low angle XRD results, TEM analysis and N_2 sorption isotherms confirm the existence of an ordered porous shape with narrow pore diameter size.

Synthesis of MCM–41 zeolite by chemical route under hydrothermal pressure process was accomplished in this work. MCM-41 had systematic uniform pore structure with hexagonal pattern arrangement. The optimum MCM-41 crystalline quality and wall thickness were produced at 110 °C and 120 °C for 72 h. This route is the promising method of illite waste synthesis to MCM-41 as can be described in the next part.

3.2. Analysis of synthesized MCM–41 (illite waste route)

The supernatant, a silica precursor which derived from a fusion of illite and NaOH, was an important solution for MCM-41 synthesis. The illite-alkali hydroxide fusion causes structural interference the breaking of unstable bonds because of dehydroxylation process. This process led to the decomposition of structure and breaking of unstable bonds at mild temperature which is corresponds to collapse of interlayers spacing of Algerian bentonite fusion in research by Adjdir et al. (2015) [32]. Water is detached from the octahedral layers by chemical dehydroxylation as described in Eqs. (1)–(2). In this research, the hydrophilic head groups of surfactant molecules and inorganic precursors are obtained by self-assembly cooperative process taking place in-situ between silica framework and templates.

$$OH^- + OH^- \longrightarrow H_2O\ (g) + O_2{}^- \tag{1}$$

$$\equiv Si{-}O{-}R + H_2O \longleftrightarrow \equiv Si{-}O{-}H + R{-}OH \tag{2}$$

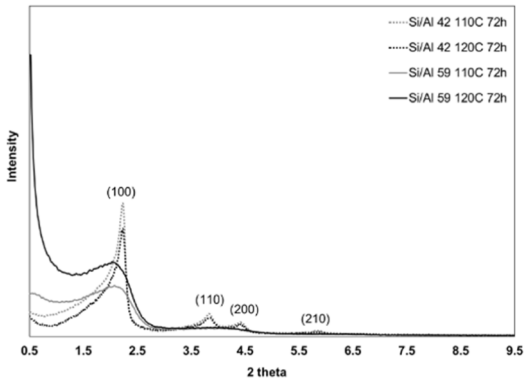

Fig. 5. XRD pattern (crystallinity) of synthesized MCM-41 (illite waste route).

Low angles XRD patterns show the peaks which associate with one strong peak at 2θ of 2.16 degree and sharp diffraction peak (d_{100}) plane. Three weak diffraction peaks at 2θ ranging of 3.74, 4.30, and 5.72 degree attributable to the reflection from (d_{110}), (d_{200}) and (d_{210}) planes, respectively. The MCM-41 catalyst samples show high-intensity peak in low-angles range 2θ as illustrated in Fig. 5. These diffraction peaks indicate the long-range ordering and mesoporous structure of MCM-41 synthesis from illite waste. Low angle XRD results identified the cell parameter "a_0" based on the 2θ position of the maximum intensity peak (d_{100}) and Bragg's Law as Eqs. (3)–(4).

$$2d_{100} \sin\theta = n\lambda \tag{3}$$

$$a_0 = (2/\sqrt{3}) \cdot d_{100} \tag{4}$$

where 'n' is an integer equal to 1. The pore structure of typical MCM-41 results from the systematic arrangement of the mesopores. Cell parameter values correspond to the center equidistant between the adjacent parallel pores [33]. The cell parameter value can provide a simple estimation of the relative size of pore diameters when comparing samples of MCM-41.

The specific surface area of the synthesized MCM-41 was calculated using the BET isotherm model, while the pore diameter distribution and pore volume were achieved by applying the Barrett–Joyner–Halenda (BJH) pore analysis as listed in Table 2. The optimum MCM-41 crystalline quality for Si/Al ratio of 42 and 59 was attained at 72 h hydrothermal holding time with the surface area of 921–952 and 670–742 m^2/g, respectively. The surface morphology of catalyst was examined by SEM. The internal morphology can be observed by TEM. The MCM-41 synthesized from illite is presented in Fig. 6. A uniform pore system and distinguish hexagonal patterns of the pores or honeycomb-like structure were proved in the results.

Table 2. Textural properties of synthesized MCM-41 catalysts (hydrothermal holding time of 72 h).

Catalyst sample	Temperature	Crystalline (%)	S_{BET} (m^2/g)	Pore volume (cm^3/g)	Pore diameter (nm)	Wall thickness (nm)
Si/Al 42	100 °C	41.52	941.30	0.92	3.91	1.74
	110 °C	57.26	951.80	0.89	3.77	1.90
	120 °C	37.33	921.50	1.04	2.74	1.93
Si/Al 59	100 °C	51.86	741.80	0.73	2.38	2.40
	110 °C	59.93	729.70	0.69	3.81	1.94
	120 °C	46.26	670.40	0.80	2.94	2.01

From previous works, natural materials such as volclay, kaolin clay, or sediment were used as alternative sources for silica and alumina. The alkali fusion process can be applied for different sedimentary rock, clay minerals and coal fly ash. Most of the synthesis process consists of sol–gel and hydrothermal [21,33]. However, the synthesis of MCM-41 by hydrothermal treatment yielded higher surface area than that of sol–gel technique. Illite is an attractive raw material due to its similarity to zeolite in terms of chemical composition. The specific surface area of MCM-41

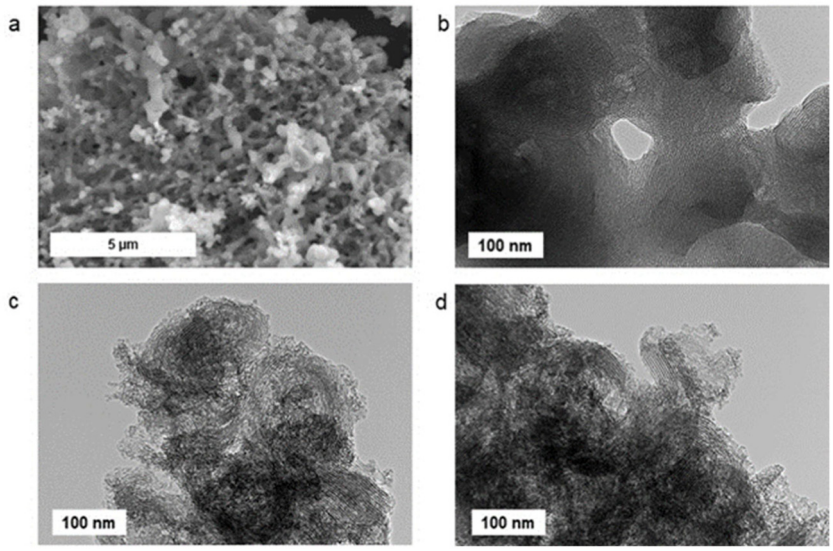

Fig. 6. SEM and TEM of MCM-41 synthesized at different conditions (a) SEM of Si/Al 42-110 °C; (b) TEM of Si/Al 42-110 °C; (c) TEM of Si/Al 59-110 °C; (d) TEM of Si/Al 59-120 °C.

from illite wastes is 952 m^2/g which is higher than results from other works which were derived from wheat ash [21], coal fly ash [22], and sediment clay [34]. It can be noted that illite waste route for MCM-41 synthesized with Si/Al ratio of 42 and hydrothermal temperature of 110 °C may be suggested as a good condition for supporter preparation.

3.3. Characterization of 5Co/MCM-41 and 5Fe/MCM-41 catalyst

For analysis of the diffraction patterns of metal-based catalysts, the high-angles range of XRD was employed. The obtained patterns for metals phases in this work are shown in Fig. 7. In this work, all metal/MCM-41 catalysts appeared in the broad amorphous of silica peak of approximately 23–27° which confirms that MCM-41 structures were stable after gasification at 800 °C [35]. Cobalt-modified catalyst has three diffraction peaks at 2θ at 36.1°, 41.2°, and 50.5° corresponding to the Co_3O_4 crystallites. Cobalt silicate formation may result from the formation of Co_3O_4 on the pore wall surface when the sample was calcined. Likewise, Cuello et al. (2013) [36] studied the structure and magnetic properties of Co/MCM-41 as magnetic nanocomposites. They found very small peaks of 10–15 wt% cobalt loading (2θ = 36.8°, 44.8°, 59.3° and 65.2°) which can be characterized by Co_3O_4 nanoparticles form. Additionally, the diffraction peaks indicating the formation of Co_2AlO_4(cobalt aluminate species) phases because the cobalt oxide species (Co^{2+} and Co^{3+}) can be generated and strongly interact with the supporter and leading to the reduction of surface Co silicate [37]. Cobalt oxide clusters and Co_3O_4 nanoparticles could be confined inside the mesoporous of MCM-41 synthesized in this research.

Iron supported MCM-41 mesoporous catalyst was prepared by incipient wetness impregnation. The four peaks diffraction of Fe-modified on MCM-41 surface are presented at 34.5°, 38.3°, 48.8°, and 62° relatively with the Fe_2O_3 crystallites. Dutt et al. (2020) [38] found that the diffraction peaks appeared at 2θ range of 24.3°, 33.2°, 35.6°, 40.6°, 49.3°, 53.1°, 62.4°, 64.0° corresponding to iron oxide in MCM-41 framework. The peaks located in the patterns are in accordance with the rhombohedral structure.

The 5Co/MCM-41 samples, indicating the increase at a relative pressure (P/P_0) ca. 0.20–0.40, are associated with capillary condensation of N_2 within narrow-pore size distribution of the MCM-41 structure as can be observed in Fig. 8. 5Fe/MCM-41 catalyst presents an ordinary type-IV isotherm with inflection at relative pressure (P/P_0) ca. 0.25–0.40, which are intrinsic properties of mesoporous materials with uniform mesopores which corresponds to the work of Cheng et al. (2020) [39]. The surface area of 5Co/MCM-41as less than 5Fe/MCM-41 catalyst. The size of cobalt oxide particles which normally in range of 3–5 nm in this research is bigger than the pore diameter size of MCM-41 which could attribute to be an agglomeration on MCM-41 surface after calcination [40]. Tran et al.

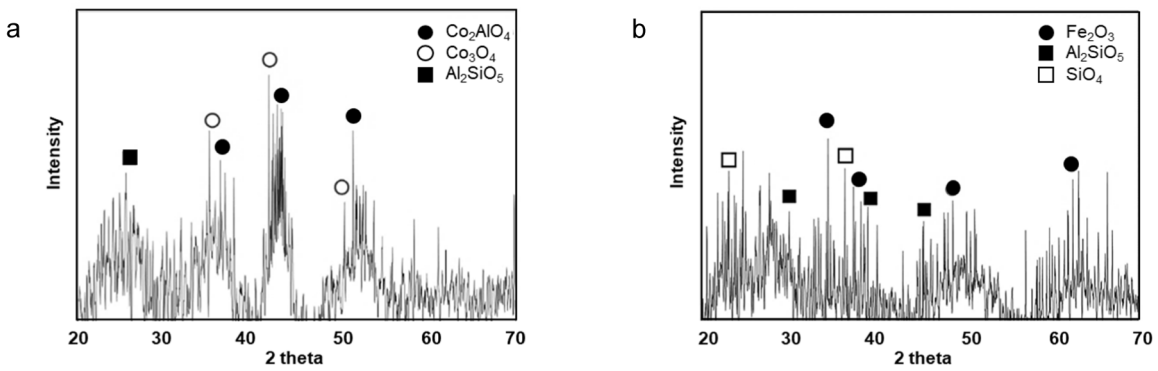

Fig. 7. Powder X-ray diffraction patterns of as-synthesized metal/MCM-41 from illite waste (a) 5Co/MCM-41; (b) 5Fe/MCM-41.

(2016) [35] found that the majority of cobalt oxide particles size were observed in range of 3–14 nm approximately. Moreover, according to the study of Rane et al. (2010) [41] reported particle sizes of the cobalt oxide varied in wide-ranging of 4.9–32.6 nm. The pore size diameter of 5Fe/MCM-41 was close to MCM-41 support sample. Because the presence of iron oxide particles located inside the MCM-41 porous were superior dispersed by the aqueous impregnation method. However, it can be noted that the porosity of the catalyst is slightly lower than that MCM-41 parent support which is considered statistically non-significant in this work (see Table 3).

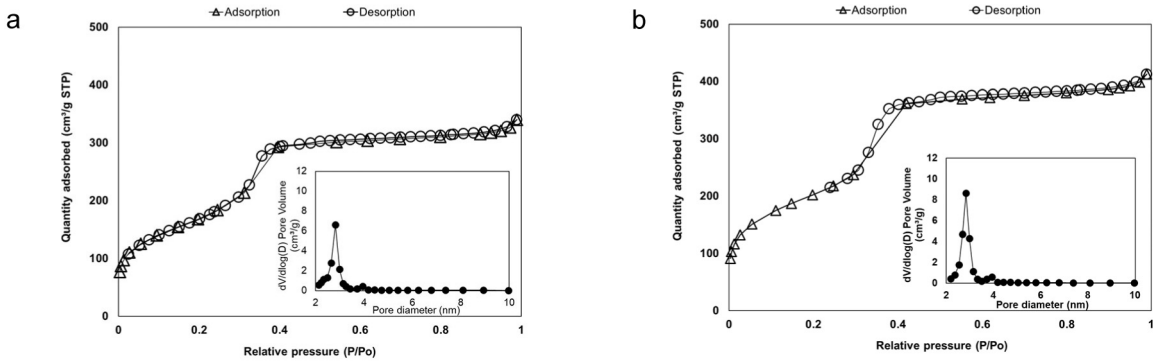

Fig. 8. N_2 physisorption isotherm and total pore volume of: (a) 5Co/MCM-41; (b) 5Fe/MCM-41.

Table 3. Characterization the textural properties of synthesized catalysts in this work.

Catalyst sample	S_{BET} (m^2/g)	Pore volume (cm^3/g)	Pore diameter (nm)
5Co/MCM-41	623.10	0.54	3.30
5Fe/MCM-41	735.73	0.69	3.40

The surface morphology of synthesized MCM-41 with adjusting the pH to 10.5–11.5 produced well-ordered structure arrangement. Cobalt oxide and iron oxide particles can be seen on the surface of MCM-41 supported, whereas some metal particles were preferentially located inside the MCM-41 pores [42,43]. On the SEM and TEM images in Fig. 9, it was appeared that all samples display the organized structure, although smaller pore size materials (<4 nm) exhibit the most typical hexagonal arrangement of uniform pores. The results derived from TEM confirmed retention of mesoporous long-range order when Co and Fe are present. Due to difference in electronic density, the bundles of darker color tone were allocated to metal oxide whilst the areas of lighter tone were MCM-41. 5Co/MCM-41 and 5Fe/MCM-41 catalysts show the same patterns of sharp capillary condensation in the same

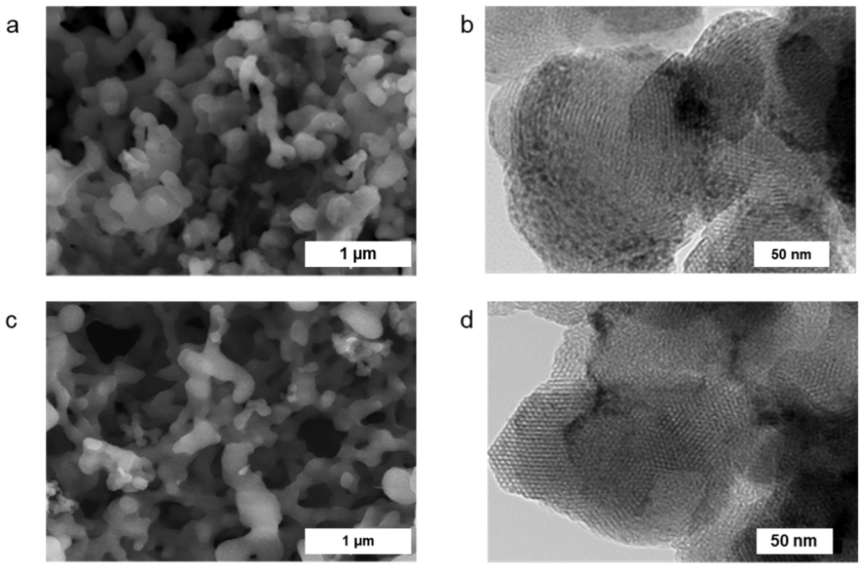

Fig. 9. Morphology images of catalyst samples (a) SEM of 5Co/MCM-41; (b) TEM of 5Co/MCM-41; (c) SEM of 5Fe/MCM-41; (d) TEM of 5Fe/MCM-41.

relative pressure range, which means that many first-row transition metals can be incorporated into the framework without structural collapse.

3.4. Catalytic gasification of TCR

TCR is suitable raw material for gasification as the major elements in TCR are carbon, hydrogen, nitrogen, sulfur, and oxygen at 55.57, 5.22, 5.50, 0.05, and 33.66 wt%, respectively. The proximate analysis of moisture, volatile, ash and fixed carbon were 5.06, 58.61, 10.45, and 25.88 wt%, respectively with heating value of 24.40 MJ/kg. For gasification trials, the investigated temperatures were 700 °C and ER of 0.4 with continuous feeding of raw material TCR at 1 g/min for 30 min. The product yields from gasification were as illustrated in (Fig. 10a). The gaseous products consist of CO, CO_2, CH_4, H_2 and other low molecular volatile hydrocarbons. During this small reaction time frame, generation of CO and H_2 gas occurs mainly from rapid pyrolysis step when TCR raw materials were fed into the reactor. During this step, the formation of CO_2 primarily originates from the cracking of carbonyl (C═O) and carboxyl (COOH) groups, while it is attributed to lignin decomposition by cracking of COOH and C–O groups on the carbohydrate [44]. Due to relatively low O/C ratio of TCR, less CO_2 is produced from the gasification. The typical degradation of carbonyl group (C═O) and ether group (C–O–C) functional groups of cellulose and hemicellulose released the CO. The majority of release of methoxy groups involved in the breaking of C–C bonds of lignin produced the CH_4 [44,45].

The product gas slightly changed in the presence of MCM-41, 5Co/MCM-41, and 5Fe/MCM-41 during the gasification process. The syngas composition from TCR gasification without catalyst experiment consisted of CO (5.61 vol.%), H_2 (2.48 vol.%), CH_4 (2.23 vol.%), C_xH_y (0.12 vol.%) and CO_2 (11.39 vol.%) while deployment of MCM-41 induced more preferred gas composition as CO_2 decreased 3 vol%. Utilizing MCM-41 catalyst yields the least liquid (9.03 wt%), whereas applying Fe/MCM-41 yields the highest liquid (12.67 wt%). However, the activity of this gasification with catalyst is also affected by factors such as conversion, heating value, or gasification efficiency. The conversion is calculated from the carbon and hydrogen in TCR that is converted to gaseous products such as CO, H_2, CO_2 and CH_4. These calculated gas conversions were illustrated in Fig. 10(b). For non-catalytic gasification, the conversion of hydrogen was 15.19% when gasified with 5Co/MCM-41 and 5Fe/MCM-41, the hydrogen conversions were improved to 22.20%, and 26.80%, respectively. CH_4 is one of the major gaseous species from gasification; it is representative of the C–H breakage which is present in hydrocarbons. Conversions of carbon are obtained at around 70.02–77.30% when gasified TCR with 5Co/MCM-41 and 5Fe/MCM-41. 5Fe/MCM-41 was better performed in terms of 26.95% carbon conversion into CO than those of MCM-41 and 5Co/MCM-41 catalysts.

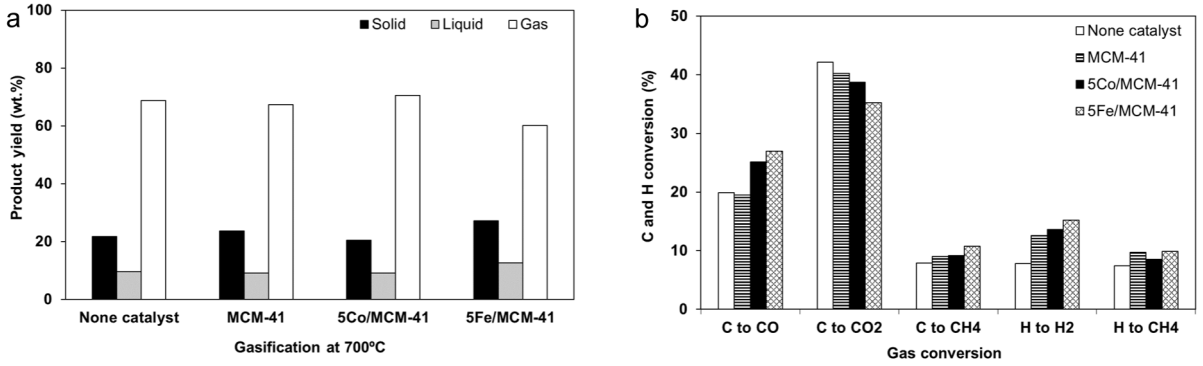

Fig. 10. The gasification TCR (a) the product yields; (b) C and H conversions.

Gasification of TCR with any metal/MCM-41 cases showed higher CO and H_2 which well corresponds to previous works [28]. Due to higher CO conversions by water–gas shift reactions effect on the decrease of CO_2 content for all catalyst experiments. The H_2/CO data yielded similar value in each of any trials due to the enlargement in the concentration of CO, because the water–gas shift reaction favors the generation of CO as illustrated in (Fig. 11a). The catalyst temperature was investigated at 500 °C which is a typical temperature of catalytic cracking of tar in the gasification process, similar to previous works with cedar wood (500 °C) and sunflower stalk (600 °C) [46,47]. The ratio of H_2 to CO required for onward process utilization depends on the intended application. The effect of Co and Fe catalytic pyrolysis of biomass at 700 °C was studied by Jaffar et al. (2019) [48], who found that their effectiveness rely on the distribution and liberation of free metal, which then becomes incorporated as a complex assemblage into the carbon structure. Likewise, Yu et al. (2011) [49] report that the release of CO_2 and CO was earlier in comparison with CH_4 and H_2, and the quantity of CO_2 and CO was stronger than CH_4 and H_2 as well. In catalytic tar cracking, the raw gas is passed over a catalyst and the tar molecules are broken down to lighter hydrocarbon gaseous. The presence of catalysts play an effective role in hydrogen conversion into H_2 and CH_4 through reforming the reactions of hydrocarbon gases as in Eqs. (5)–(7). Decomposition of volatile and hydrocarbon during gasification of TCR is more prominent than others since volatiles react with themselves in the gas–gas phase reactions. Loss of water and volatiles in TCR can be obtained in the gas phase. These are explained in gas-phase phenomena of volatile gases released during gasification. In gas phase reactions include the dry reforming of methane, CO_2 hydrogenation, the water–gas shift reaction is various chemical process for increasing the H_2 in syngas, while the methanation influences the CH_4 product. The Boudouard reaction converts CO_2 into CO. At temperatures below 1000 °C, this reaction would be in equilibrium and the CO remains in the synthesized gas.

$$CO + H_2O \rightleftharpoons CO_2 + H_2 \tag{5}$$

$$CH_4 + H_2O \rightleftharpoons CO + 3H_2 \tag{6}$$

$$C_xH_y + xH_2O \rightleftharpoons xCO + (x + y/2)H_2 \tag{7}$$

The lower heating value (LHV) of the gas products and cold gas efficiency (CGE) calculated from this experimental. CGE, the worldwide factor can be used to estimate the overall performance of the gasifier and biomass type. These results are directly related to gas products yield and biomass heating value. The LHV of product gas reach about 9.26 MJ/kg and 10.72 MJ/kg with the use of 5Co/MCM-41 and 5Fe/MCM-41 catalysts, respectively, indicating a good quality of the synthesized gas from catalytic gasification of TCR. CGE is calculated from the ratio between the chemical energy of the produced gas and the feeding biomass energy content as shown in Fig. 11(b). The maximum efficiencies are 43.27 and 50.11% when using 5Co/MCM-41 and 5Fe/MCM-41, respectively. This result is owning to the higher CH_4 content in syngas. However, CGE can be tuned within each of the individual gasifier designs such as, higher carbon conversion into CO while lower CH_4 conversion.

Generally, 5Co/MCM-41 is preferred over 5Fe/MCM/41 and MCM-41 for its higher activity such as better stability in deactivation, lower liquid production and lower selectivity to the water–gas shift reaction. The CO_2 was low for all the catalysts and decreases at higher CO conversions in accordance with water–gas shift reaction. The

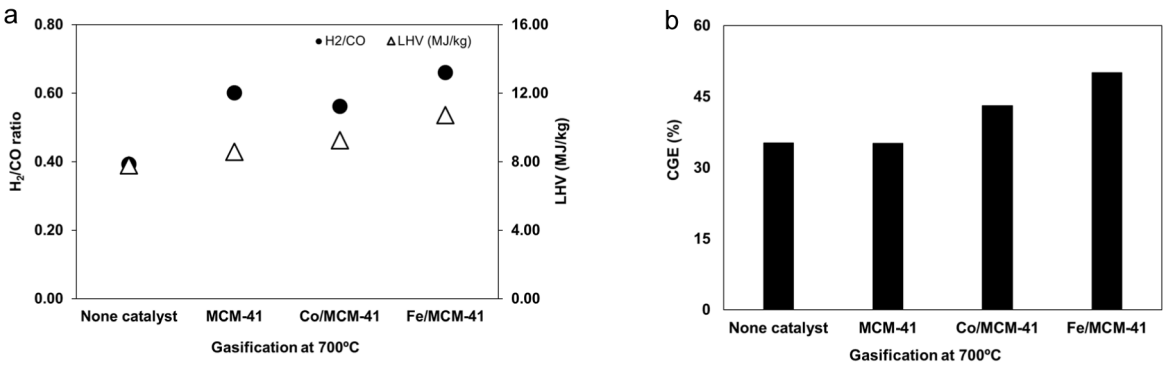

Fig. 11. Performance of TCR gasification: (a) H_2/CO and LHV; (b) cold gas efficiency.

addition of 5Co/MCM-41 and 5Fe/MCM-41 catalysts in the second stage enhanced the CO, H_2 and CH_4 conversion, tar reduction and CGE with higher LHV.

4. Conclusions

MCM-41 mesoporous was successfully prepared using illite clay waste as the silica and alumina source by an alkali fusion followed hydrothermal technique. The physical properties of MCM-41 synthesized by illite waste present the hexagonal ordered structure with a higher specific surface area. The effect of parameters for MCM-41 synthesis by illite waste were Si/Al ratio in raw material, temperature, aging time, water, and pH adjustment. Catalytic gasification of TCR with synthesized catalysts was effectively conducted at temperatures of 700 °C and ER of 0.4 in which 5Fe/MCM-41catalyst showed outstanding activity with the highest conversion to H_2 and good gas heating value. Both Co/MCM-41 and 5Fe/MCM-41 performed better than MCM-41 supporter and may be used in a secondary reactor of the gasifier for tar removing and gas upgrading. The decent property of obtained fuel gas, especially the lower heating value of gas and species distribution implies that it can be effectively burnt as a quality fuel gas e.g., in a boiler for heat, or in an electricity generation or combined heat and power process. Further research should be the torrefaction of others biomass such as, para rubber seed meal, Pongamia pinnata waste, or water hyacinth for subsequently gasification process.

Declaration of competing interest

The authors declare that they have no known competing financial interests or personal relationships that could have appeared to influence the work reported in this paper.

Acknowledgment

This research was supported by the National Metal and Materials Technology Center (MTEC), Thailand [Project No. MT-ICF-61-POL-07-593-I].

References

[1] Nattapong Kongprasert, Pilada Wangphanich, Anuwat Jutilarptavorn. Charcoal briquettes from madan wood waste as an Alternative Energy in Thailand. Procedia Manuf 2019;30:128–35.

[2] Krongkaew Laohalidanond, Palita Chaiyawong, Somrat Kerdsuwan. Status of using biomass gasification for Heat and Power in Thailand. Energy Procedia 2015;79:385–90.

[3] Wei-Hsin Chen, Bo-Jhih Lin, Yu-Ying Lin, Yen-Shih Chu, Ubando Aristotle T, Pau Loke Show, et al. Progress in biomass torrefaction: Principles, applications and challenges. Prog Energy Combust Sci 2021;82:100887.

[4] Yen-Hau Chen, Chia-Chi Chang, Ching-Yuan Chang, Min-Hao Yuan, Dar-Ren Ji, Je-Lueng Shie, et al. Production of a solid bio-fuel from waste bamboo chopsticks by torrefaction for cofiring with coal. J Anal Appl Pyrol 2017;126:315–22.

[5] Shih-Hsin Ho, Congyu Zhang, Wei-Hsin Chen, Ying Shen, Jo-Shu Chang. Characterization of biomass waste torrefaction under conventional and microwave heating. Bioresour Technol 2018;264:7–16.

[6] Jinwen Hu, Yueyao Song, Jingyong Liu, Fatih Evrendilek, Musa Buyukada, Youping Yan, et al. Combustions of torrefaction-pretreated bamboo forest residues: Physicochemical properties, evolved gases, and kinetic mechanisms. Bioresour Technol 2020;304:122960.
[7] Thossaporn Onsree, Nakorn Tippayawong. Analysis of reaction kinetics for torrefaction of pelletized agricultural biomass with dry flue gas. Energy Rep 2020;6:61–5.
[8] Yu Liu, Emad Rokni, Ruilei Yang, Xiaohan Ren, Rui Sun, Levendis Yiannis A. Torrefaction of corn straw in oxygen and carbon dioxide containing gases: Mass/energy yields and evolution of gaseous species. Fuel 2021;285:119044.
[9] Congyu Zhang, Shih-Hsin Ho, Wei-Hsin Chen, Youping Xie, Zhenquan Liu, Jo-Shu Chang. Torrefaction performance and energy usage of biomass wastes and their correlations with torrefaction severity index. Appl Energy 2018;220:598–604.
[10] Ram Nhuchhen Daya, Afzal Muhammad T. HHV predicting correlations for torrefied biomass using proximate and ultimate Analyses. Bioengineering 2017;4(1):7.
[11] Arkadiusz Dyjakon, Tomasz Noszczyk, Smędzik. The influence of torrefaction temperature on hydrophobic properties of waste biomass from food processing. Energies 2019;12:4609.
[12] Quang-Vu Bach, Ngoc Trinh Trung, Khanh-Quang Tran, Dung Thi Ngoc Bao. Pyrolysis characteristics and kinetics of biomass torrefied in various atmospheres. Energy Convers Manage 2017;141:72–8.
[13] Almeida A, Pilão R, Ramalho E, Ribeiro A, Pinho C. Co-gasification of glycerol/fat mixtures in a downflow fixed bed reactor: Preliminary results. Energy Rep 2020;6:460–5.
[14] Akanksha Mishra, Shalini Gautam, Tripurari Sharma. Effect of operating parameters on coal gasification. Int J Coal Sci Technol 2018;5(2):113–25.
[15] Zhihui Yu, Yu Wang, Xiaoyu Liu, Jiangbo Sun, Guangyan Sha, Jinhui Yang, et al. A novel pathway for the synthesis of ordered mesoporous silica from diatomite. Mater Lett 2014;119:150–3.
[16] Mahsa Foroughi, Amin Salem, Shiva Salem. Characterization of phase transformation from low grade kaolin to zeolite LTA in fusion technique: Focus on quartz melting and crystallization in presence of $NaAlO_2$. Mater Chem Phys 2021;258:123892.
[17] Hamadi A, Nabih K. Synthesis of Zeolites Materials using Fly Ash and oil shale ash and their applications in Removing Heavy Metals from aqueous solutions. J Chem 2018;2018:6207910.
[18] Wahyu Purnomo Chandra, Chris Salim, Hirofumi Hinode. Synthesis of pure Na–X and Na–A zeolite from bagasse fly ash. Microporous Mesoporous Mater 2012;162:6–13.
[19] Guo Lin, Qiang Zhuang, Qun Cui, Haiyan Wang, Huqing Yao. Synthesis and adsorption property of zeolite FAU/LTA from lithium slag with utilization of mother liquid. Chin J Chem Eng 2015;23(11):1768–73.
[20] Abdelrahman Ehab A. Synthesis of zeolite nanostructures from waste aluminum cans for efficient removal of malachite green dye from aqueous media. J Molecular Liquids 2018;253:72–82.
[21] Sohrabnezhad Sh, Jafarzadeh A, Pourahmad A. Synthesis and characterization of MCM-41 ropes. Mater Lett 2018;212:16–9.
[22] Dandan Li, Hongyang Min, Xu Jiang, Xianqiang Ran, Liyin Zou, Jianwei Fan. One-pot synthesis of aluminum-containing ordered mesoporous silica MCM-41 using coal fly ash for phosphate adsorption. J Colloid Interface Sci 2013;404:42–8.
[23] Chunyan Sun, Feng Zhang, Xiao Wang, Fangqin Cheng. Facile preparation of Ammonium molybdophosphate/Al-MCM-41 composite material from natural clay and its use in Cesium Ion adsorption. Eur J Inorg Chem 2015;12(2015):2125–31.
[24] Guang Yang, Yanxi Deng, Jie Wang. Non-hydrothermal synthesis and characterization of MCM-41 mesoporous materials from iron ore tailing. Ceram Int 2014;40(5):7401–6.
[25] Roman Jaskulski, Daria Jóźwiak-Niedźwiedzka, Yaroslav Yakymechko. Calcined clay as supplementary cementitious material. Materials 2020;13(21):4734.
[26] Nishant Garg, Jørgen Skibsted. Pozzolanic reactivity of a calcined interstratified illite/smectite (70/30) clay. Cem Concr Res 2016;79:101–11.
[27] Irassar Edgardo F, Bonavetti Viviana L, Cristina Castellano C, Trezza Monica A, Rahhal Viviana F, Gisela Cordoba, et al. Calcined illite-chlorite shale as supplementary cementing material: Thermal treatment, grinding, color and pozzolanic activity. Appl Clay Sci 2019;179:105143.
[28] Peng Lu, Qunxing Huang, Bourtsalas Athanasios C, Yong Chi, Jianhua Yan. Effect of operating conditions on the coke formation and nickel catalyst performance during cracking of Tar. Waste Biomass Valoriz 2019;10(1):155–65.
[29] Subhashish Dey, Chandra Dhal Ganesh, Devendra Mohan, Ram Prasad, Nayan Gupta Rajeev. Cobalt doped CuMnOx catalysts for the preferential oxidation of carbon monoxide. Appl Surf Sci 2018;441:303–16.
[30] Zamboni I, Courson C, Kiennemann A. Fe-Ca interactions in Fe-based/CaO catalyst/sorbent for CO2 sorption and hydrogen production from toluene steam reforming. Appl Catal B 2017;203:154–65.
[31] Punchaluck Sirinwaranon, Duangduen Atong, Viboon Sricharoenchaikul. Gasification of torrefied cassava rhizome with Ni/MCM-41 catalyst derived from illite waste. Energy Rep 2020;6:537–47.
[32] Mehdi Adjdir, Bendeddouche Choukry K, Hadj Benhaoua, Mhamed Kaid, Mohamed Karmaoui, Mohamed Boudinar, et al. Increasing the efficiency of silicon and aluminum extraction from volclay by a water iteration treatment for the synthesis of MCM-41 nanomaterials. C R Chim 2015;18(4):385–90.
[33] Kresge CT, Leonowicz ME, Roth WJ, Vartuli JC, Beck JS. Ordered mesoporous molecular sieves synthesized by a liquid-crystal template mechanism. Nature 1992;359(6397):710–2.
[34] Boldrini Diego E, Sabrina Angeletti, Cervellini Patricia M, Reinoso Deborath M. Highly ordered mesoporous Al-MCM-41 synthesis through valorization of natural sediment. ACS Sustain Chem Eng 2019;7(5):4684–91.
[35] Nga Tran, Yoshimitsu Uemura, Sujan Chowdhury, Anita Ramli. Vapor-phase hydrodeoxygenation of guaiacol on Al-MCM-41 supported Ni and Co catalysts. Appl Catal A 2016;512:93–100.
[36] Cuello N, Elías V, Crivello M, Oliva M, Eimer G. Synthesis, characterization and magnetic behavior of Co/MCM-41 nano-composites. J Solid State Chem 2013;205:91–6.

[37] Yan Hao, Qin Hansong, Liang Wei, Jin Xin, Zhang Yashuang, Feng Xiang, Liu Yibin, Chen Xiaobo, Yang Chaohe. Enhanced performance of bimetallic PtCo/MCM-41 catalysts for glycerol oxidation in base-free medium. Catal Sci Technol 2019;9(18):4909–19.
[38] Meenakshi Dutt, Ayushi Kaushik, Monika Tomar, Vinay Gupta, Vaishali Singh. Synthesis of mesoporous α-Fe2o3 nanostructures via nanocasting using MCM-41 and KIT-6 as hard templates for sensing volatile organic compounds (VOCs). J Porous Mater 2020;27.
[39] Shang-Yuan Cheng, You-Zhi Liu, Gui-Sheng Qi. Microwave synthesis of MCM-41 and its application in CO_2 absorption by nanofluids. J Nanomater 2020;2020:6187656.
[40] Thulani Nyathi, Nico Fischer, Andrew York, David Morgan, Graham Hutchings, Emma Gibson, et al. Impact of nanoparticle-support interactions in Co_3O_4/Al_2O_3 catalysts for the preferential oxidation of carbon monoxide. ACS Catal 2019;9:7166–78.
[41] Shreyas Rane, Øyvind Borg, Jia Yang, Erling Rytter, Anders Holmen. Effect of alumina phases on hydrocarbon selectivity in Fischer–Tropsch synthesis. Appl Catal A 2010;388(1):160–7.
[42] Samson Akpotu, Brenda Moodley. Application of as-synthesised MCM-41 and MCM-41 wrapped with reduced graphene oxide/graphene oxide in the remediation of acetaminophen and aspirin from aqueous system. J Environ Manag 2017;209:205–15.
[43] Chunfei Wu, Leizhi Wang, Williams Paul T, Jeffrey Shi, Jun Huang. Hydrogen production from biomass gasification with Ni/MCM-41 catalysts: Influence of Ni content. Appl Catal B 2011;108–109:6–13.
[44] Yuan Liu, Feiqiang Guo, Xiaolei Li, Tiantao Li, Kuangye Peng, Chenglong Guo, et al. Catalytic effect of iron and nickel on gas formation from fast biomass pyrolysis in a microfluidized bed reactor: A kinetic study. Energy Fuels 2017;31(11):12278–87.
[45] Zhen-Yi Du, Xia Wang, Yu-Hong Qin, Zhi-Hua Zhang, Jie Feng, Wen-Ying Li. Effects of secondary reactions on the destruction of cellulose-derived volatiles during biomass/coal co-gasification. Energy Fuels 2016;30(2):1145–53.
[46] Surachai Karnjanakom, Guoqing Guan, Bayu Asep, Xiao Du, Xiaogang Hao, Chanatip Samart, et al. Catalytic steam reforming of tar derived from steam gasification of sunflower stalk over ethylene glycol assisting prepared Ni/MCM-41. Energy Convers Manage 2015;98:359–68.
[47] Chunfei Wu, Lisha Dong, Jude Onwudili, Williams Paul T, Jun Huang. Effect of Ni particle location within the mesoporous MCM-41 support for Hydrogen Production from the Catalytic Gasification of biomass. ACS Sustain Chem Eng 2013;1(9):1083–91.
[48] Jaffar Mohammad M, Nahil Mohamad A, Williams Paul T. Methane production from the pyrolysis–catalytic hydrogenation of waste biomass: Influence of process conditions and catalyst type. Energy Fuels 2019;33(8):7443–57.
[49] Jian Yu, Changbin Yao, Xi Zeng, Shuang Geng, Li Dong, Yin Wang, et al. Biomass pyrolysis in a micro-fluidized bed reactor: Characterization and kinetics. Chem Eng J 2011;168(2):839–47.